

Electrocatalytic Hydrogen Generation using Sn loaded TiO₂ Nanotubes

Khadijah M. Emran*, Rawan M. A. Alsahli

Department of Chemistry, College of Science, Taibah University, Madinah 30002, KSA

*E-mail: kabdalsamad@taibahu.edu.sa

Received: 28 January 2021 / Accepted: 20 March 2021 / Published: 30 April 2021

Advanced nanomaterials for electrocatalytic water splitting are crucial to the field of renewable energy. Here, we developed a novel hydrothermal synthesis of tin-titanium oxide nanotubes (Sn-TNTs) selectively on GC electrodes in acidic solution. XRD, SEM, EDX, and Raman spectra characterizations of TNT and doped Sn-TNTs were carried out, suggesting successful incorporation of Sn in the tubular structure of TiO₂. The catalytic activity towards the hydrogen evolution reaction (HER) of TNTs and Sn-TNTs doped with electrodeposited Pd and/or Pt nanoparticles was investigated using CV and Tafel polarization measurements. The activation energy (E_a) and reaction mechanism were determined using Tafel polarization curves. The Sn-TNTs/Pt-Pd-modified catalyst showed greater efficiency and lower E_a (2.78 kJ/mol) for the electrocatalytic production of hydrogen than the Sn-TNTs, where no activity has been shown with TNTs. Adsorption of hydrogen on the catalyst controlled the overall reaction rate. This study opens a new viewpoint for the development of highly active TNT electrocatalysts for hydrogen production from water splitting.

Keywords: titania; hydrothermal synthesis; nanotube; water splitting; energy.

1. INTRODUCTION

Titanium oxide (TiO₂) has effective catalytic activity as well as a low cost, good stability in electrochemical environments, strong metal support interactions, high corrosion resistivity towards aqueous media, and good proton conductivity [1-4]. One-dimensional (1-D) titanium oxide nanotubes (TNTs) can be obtained via a hydrothermal method. This method combines a high concentration of NaOH and pure TiO₂ powder at high temperatures (over 100 °C). Dilute HCl solutions are subsequently added, resulting in the production of spaghetti-like crystalline nanotubes [5-7]. The hydrothermal product is $X_2Ti_2O_5 \cdot H_2O$, in which X can be either H or Na [3]. Although TiO₂ shows promise due to its high surface-to-volume ratio, TNTs have a wide band gap ($E_g = 3.0\sim 3.2$ eV) and low electronic conductivity. Many efforts have been applied towards narrowing the band gap, one of which was insertion of foreign elements as dopants in the TNT lattice or through atomic layer

deposition. These foreign elements are crucial for improving and modifying band edge states between the conduction band and valence band.

For clean hydrogen fuel production, doped TNTs are likely components of cathodes in future water electrolysis systems for the hydrogen evolution reaction (HER). The first report of electrochemical photolysis of water to generate hydrogen using a TiO_2 electrode was in 1972 [7]. Since that time, production of tubular TiO_2 structures has become one of the most promising routes to secure an alternative energy source. Approaches for improving the HER performance of doped TNTs have been developed. CdS quantum dots were deposited on the surface TiO_2 nanorod/ TiO_2 nanotube array (TNRs/TNTAs). The photoelectrocatalytic hydrogen production activities of CdS/TNRs/TNTs exhibited excellent stability in aqueous solutions containing Na_2S and Na_2SO_3 under visible light [8]. In the same field, versatile photocatalysts composed of SrTiO_3 /TNTs and N-doped TNTs modified with Pt by photodeposition were prepared by a hydrothermal method. The study shows that Pt/TNTs are an efficient solar light-responsive multijunction photocatalyst for hydrogen evolution [9]. Reddy *et al.* prepared Cu/Ag@TNT by a photodeposition method. The synthesized photocatalyst was activated by the UV and visible wavelengths of solar light [10]. Elezovića *et al.* developed a two-step procedure for the production of TNT arrays by Pd nanoparticles on the walls of cathodically hydrogenated TiO_2 nanotube arrays (TNTA). The Pd@TNTAs display remarkable HER activity in $1.0 \text{ mol L}^{-1} \text{ HClO}_4$, which can be ascribed to the Pd deposits and the large surface area of the TNTAs, which ensures the integrity of the Pd catalytic sites [11]. Similar to the above works, Dubey *et al.* reported the synthesis of Cu_2O nanoparticles modified vertically with TNTAs and their multifunctional application for enhanced photoelectrochemical hydrogen generation in $1.0 \text{ mol L}^{-1} \text{ Na}_2\text{SO}_4$ electrolyte solution [12]. In our previous work, we successfully prepared Nd-Gd-Pt-TNTAs [13] and Sr-TNTs [14] with a low activation energy for hydrogen production in $0.1 \text{ mol L}^{-1} \text{ H}_2\text{SO}_4$.

This paper intends to analyze hydrothermally synthesized TNT and an in situ monodoped Sn-TNT catalyst in an anatase framework as efficient electrocatalysts for decreasing the overpotential and improving the energy conversion efficiency of the hydrogen evolution reaction in water splitting processes. To our knowledge, this is the first time that hydrothermal synthesis of Sn-TNTs has been performed for hydrogen production, and that the activation energy of gas generation was calculated by an electrochemical method.

Among the metal oxides, tin dioxide (SnO_2) is a high-capacity material and has extensive applications because it typically displays low oxygen vacancy formation energy and valence variation [15-18]. Therefore, SnO_2 and Sn-doped materials have been widely utilized in batteries [19,20], NO and CO_2 [21], H_2S_2 [22] gas sensors, and catalysis [23]. Many previous studies on Sn-doped TiO_2 nanomaterials focused on the modification of the electronic and textural properties of TiO_2 nanomaterials for the photocatalytic degradation of 2,4-dichlorophenoxyacetic acid [24,2015], rhodamine B (RhB) [25, 26], and diethylsulfide (DES) [27]. These materials have been used for photocatalytic hydrogen production reactions under simulated solar light [26], and have served as efficient catalysts for dichloromethane decomposition [28] and superior anode materials for sodium ion batteries [17].

The highest electrocatalytic activity, however, is seen in the activation energy for the hydrogen evolution reaction. The activity of a catalyst is strongly affected by supported metal (Pt, Ir, Rh, Pd) nanoparticles [29-31]. According to a typical ‘volcano plot’ of the hydrogen adsorption energy of some

metals, strong metal–hydrogen (Mo, Ni, etc.) bonds could impede hydrogen atom release from the active sites as compared to Pt group metals [32]. This makes Pd and Pt suitable candidates for catalysts in the hydrogen evolution reaction.

To determine whether such supported metals (Pt and/or Pd) influence hydrogen atom release, we carried out systematic studies on the effects of supported metal on hydrogen discharge, and a mechanism was presented. The activation energy E_a was derived using thermodynamic studies. In this work, we report the related data for HER at GCEs modified by TNTs and Sn-TNTs in the absence and presence of supporting metals (Pt and/or Pd) in 0.1 mol L⁻¹ H₂SO₄.

2. EXPERIMENTAL

2.1. Chemicals/Materials

Titanium oxide (titania) TiO₂ nanopowder (P25, 99.5%, 21 nm), sodium hydroxide, NaOH, tin(II) chloride, SnCl₂, palladium(II) chloride (99%), platinum(II) chloride (99%), sulfuric acid, H₂SO₄, and N,N-dimethyl formamide (DMF) (99%) were purchased from Sigma-Aldrich, USA. HCl for the acid washing process was purchased from Marck, USA. All solutions were prepared using high-purity deionized water (DI, Milli-Q water (resistivity of 17 MΩ)). A glassy carbon (GC) electrode (3 mm diameter, eDAQ) disk was used as the working electrode. The auxiliary electrode was a platinum coil, and the reference electrode was a 3.5 mol L⁻¹ Ag/AgCl/KCl_{sat} electrode purchased from Hanna.

2.2. Synthesis of TiO₂ Nanotubes

TNTs were synthesized using the hydrothermal method proposed by previous studies [4, 33-35]. In a typical procedure, 0.5 g of TiO₂ nanopowder was dispersed in 30 mL of 10 M NaOH solution, followed by stirring for 30 min. A hydrothermal treatment of the mixture was performed at high pressure at 180 °C. After alkaline treatment, the solid precipitate was protonated by 0.1 mol L⁻¹ HCl. The sample was then filtered and dried overnight at 90 °C and calcinated at 400 °C for 2 h. For Sn-doped TNTs, reactive SnCl₂ and TiO₂ were mixed. The molar ratio of titanium to metal was 20:5. Then, the hydrothermal treatment was carried out in the same manner as the undoped titanium nanotubes.

2.3. Morphology and Component Composition

Scanning electron microscopy (SEM) images and energy-dispersive spectroscopy (EDX) data of TNTs and Sn-TNTs were obtained with a field emission JEOL-JSM-6360 instrument, USA. The crystal structure of the catalysts was studied by X-ray powder diffraction (XRD, Shimadzu, XRD-7000, Japan) from $2\theta = 20^\circ$ to 80° at 40 kV with CuK α radiation ($\lambda = 0.15406$ nm). Raman spectra were obtained with a Raman spectrometer (Sentarra, Bruker, USA) coupled to a Leica microscope

(Olympus BX series, USA) using 532 nm excitation radiation. The spectral resolution was set to 4.0 cm^{-1} .

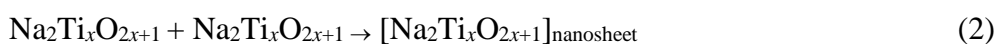
2.4. Hydrogen Generation Activity Evaluation

The electrochemical hydrogen evolution reaction was carried out using a standard three-electrode system on a potentiostat/galvanostat (Gamry interface 1000 potentiostat). The working electrode was prepared by casting 6 μL of the catalyst on a GC electrode (GCE/catalyst). Then, the working electrode was coated by a support catalyst (Pd and/or Pt) by applying a double potential step to produce a GC/catalyst/supported metal electrode. The geometric area of the GCE was calculated to be 0.0706 cm^2 , which was used to determine the current density in linear polarization measurements and cyclic voltammetry (CV) experiments at a scan rate of 100 mV s^{-1} . The activity of the electrochemical hydrogen evolution reaction was studied in 0.1 mol L^{-1} H_2SO_4 solution.

3. RESULTS AND DISCUSSION

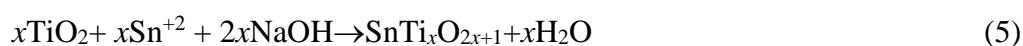
3.1. Surface Characterization

The SEM images in Fig. 1 show that the TiO_2 (P25) spherical particles (Fig. 1,a) were successfully converted into titanate nanotubes (TNTs, Fig. 1,b) and in situ tin-doped nanotubes (Sn-TNTs, Fig. 1,c) by the hydrothermal method with calcination at 400 $^\circ\text{C}$. The approximate compositions were 46.56% O_2 and 53.44% Ti for TiO_2 (P25) and 49.91% O_2 and 50.09% Ti for TNTs. The conversion mechanism from partials to tubular structures might be explained as follows:



The hydrothermal process in a strongly basic environment (10 mol L^{-1} NaOH) caused the TiO_2 particles to dissolve through a dissolution/recrystallization reaction and breakage of the Ti–O–Ti bonds to form Na–O–Ti bonds, as shown in Eq. (1). Because of the concentrated NaOH [36], Na–O–Ti bonds formed $[\text{Na}_2\text{Ti}_x\text{O}_{2x+1}]_{\text{nanosheets}}$, as shown in Eq. (2). To decrease the surface energy, the sheets rolled up and subsequently formed $[\text{Na}_2\text{Ti}_x\text{O}_{2x+1}]_{\text{nanotubes}}$, as shown in Eq. (3). Finally, rolling becomes more crucial when the sample is treated with dilute acid. H^+ ions replaced Na^+ during acid washing, resulting in $[\text{H}_2\text{Ti}_x\text{O}_{2x+1}]_{\text{nanotubes}}$, as shown in Eq. (4) [37-39].

The chemical reaction between Sn^{2+} ions can be described as follows:



During the hydrothermal process, Sn^{2+} ions could react with TiO_2 nanotubes to form $[\text{SnTi}_x\text{O}_{2x+1}]$ nanotubes through Eq. (5) via an electrostatic interaction between SnO_2 and TiO_2 . According to the EDX patterns, uniform distributions of Sn in the TNT lattice (53.42% O₂, 77.75% Ti, and 1.38% Sn) were observed.

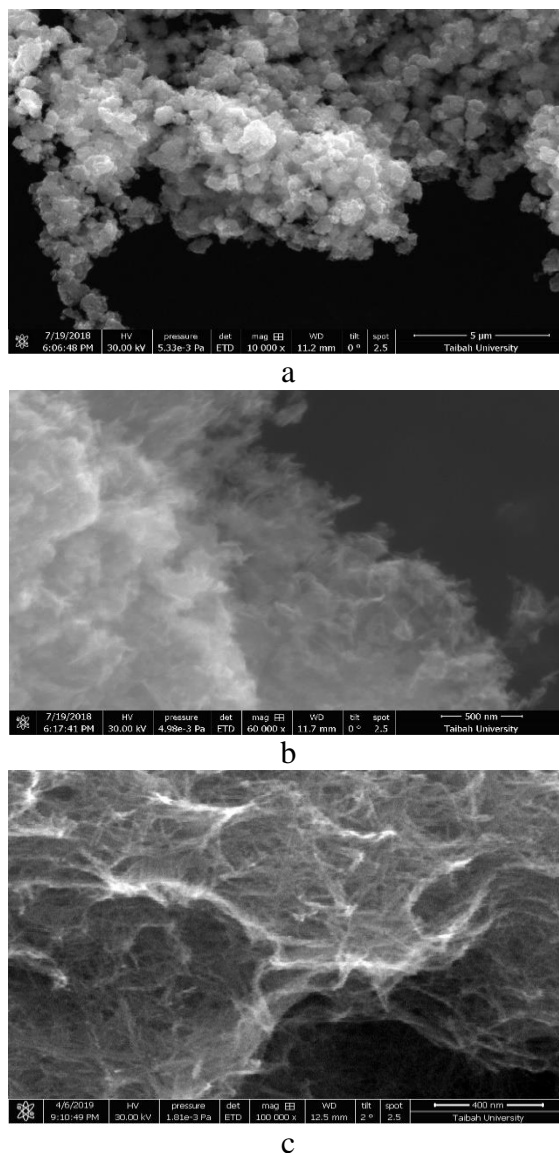


Figure 1. Surface morphology of (a) P25 TiO_2 ; (b) TNT $[\text{H}_2\text{Ti}_x\text{O}_{2x+1}]$ nanotube; (c) Sn-TNT $[\text{SnTi}_x\text{O}_{2x+1}]$ nanotube.

To further confirm the existence of Sn in TNTs in the hybrid nanomaterials, XRD experiments were employed for the structural analysis of the hybrid nanostructures (Fig. 2a). XRD results illustrate that after annealing at 400 °C for 2 h, undoped TNTs and doped Sn-TNTs are converted to anatase phases with a high degree of crystallinity. According to the standard JCPD card (00-021-1272), the diffraction peaks at 25.3°, 37.8°, 48.0°, and 55.1° of 2θ are attributed to the (101), (004), (200), and (211) anatase planes of TNT, respectively [24]. The XRD pattern of Sn-TNT indicates that the hybrid nanostructures are composed of SnO_2 and TiO_2 , and the resulting diffraction peaks located at 2θ values of 25.72°, 31.31°, and 42.18° are attributed to the (110), (111), and (121) planes of Sn^{4+} nanoparticles,

respectively. Doping with SnO₂ is ideal because the ionic radii of Sn⁴⁺ and Ti⁴⁺ are very similar (0.690 Å and 0.605 Å, respectively), meaning that Ti⁴⁺ can be easily replaced by Sn⁴⁺ in the crystal tubular structure of TiO₂ [24,40].

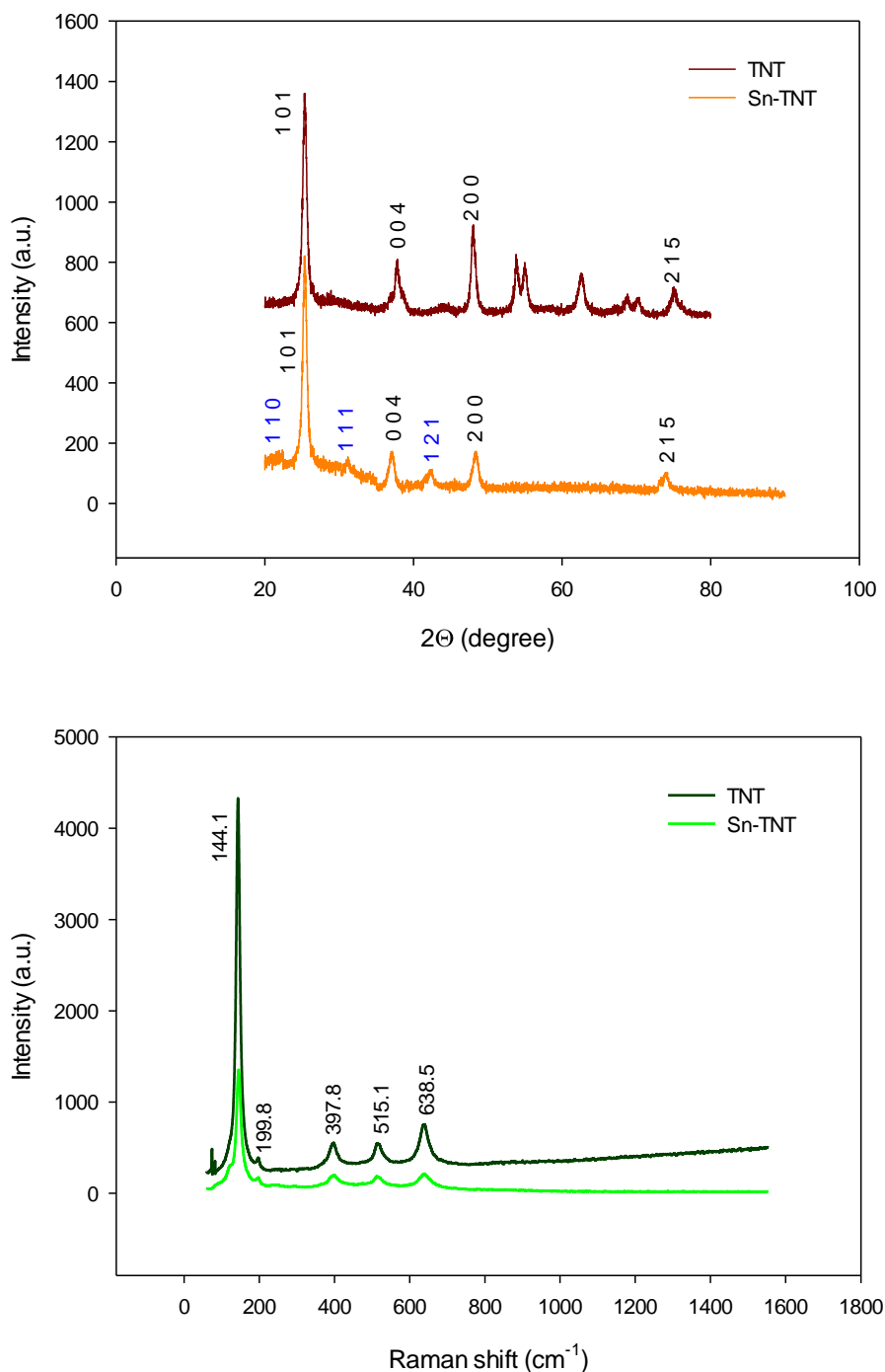


Figure 2. (a) XRD pattern and (b) Raman spectra of TNT and Sn-TNT.

The crystallographic structures of the calcined undoped TNTs and hybrid nanomaterial Sn-TNTs were analyzed by Raman spectroscopy, as shown in Fig. 2b. The Raman bands for the anatase

TNT and Sn-TNT phases at 143.1 (E_g), 198.8 (E_g), 398.8 ($B1_g$), 515.1 ($B1_g$), and 639.5 cm^{-1} , according to the three symmetry group analysis modes ($A1_g$; $2B1_g$; $3E_g$), were clearly observed [41]. The Raman spectrum does not detect the main vibration bands of SnO_2 (776 cm^{-1} , 636 cm^{-1} , 547 cm^{-1} , and 490 cm^{-1}) [42] due to the incorporation of Sn^{4+} into the TiO_2 lattice.

3.2. Electrocatalytic Hydrogen Production Activity

Catalytic activity measurements were carried out in 0.1 mol L^{-1} H_2SO_4 at room temperature. The motivation for utilizing the Sn-doped catalyst was to improve the reduction current response and limit the overpotential. Electrochemical hydrogen reduction on the TNT catalyst was investigated with cyclic voltammetry by sweeping the potential from -5.0 to 1.8 V at a scan rate of 100 mV s^{-1} in 0.1 mol L^{-1} H_2SO_4 solution (Fig. 3).

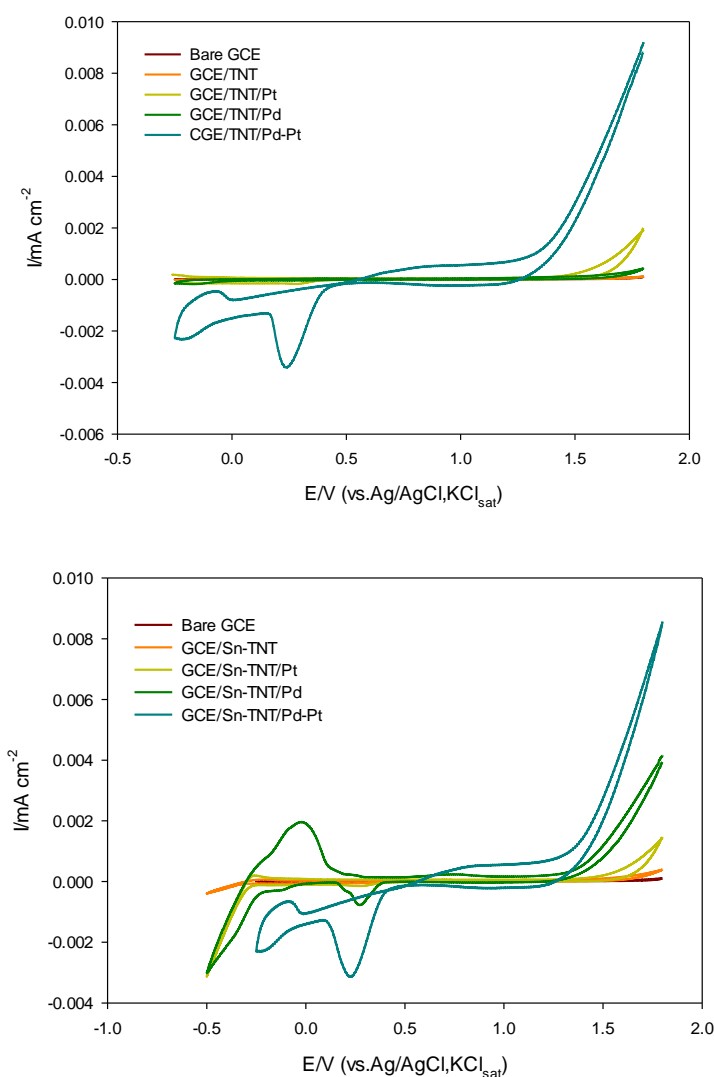


Figure 3. Cyclic voltammogram at scan rate 100 mV/s in 0.1 mol L^{-1} H_2SO_4 solution on GC electrode modified with all kinds of (a) TNTs; (b) Sn-TNTs catalysts.

The reduction peak current and peak potential were determined from the 5th cycle as they reached a steady value and are listed in Table 1. Cyclic voltammetry of the bare GC electrode was used as a control to determine any activity of the electrodes before modification by TNTs in 0.1 mol L⁻¹ H₂SO₄ solution. These data demonstrate that hydrogen was not electroreduced on the bare GC electrode. A small reductive peak of 0.056 mA cm⁻² at 0.280 V was observed for the Sn-TNT catalyst (Fig. 3b, Table 1), whereas no peak was observed for the undoped TNTs under the same conditions (Fig. 3a). There are signs of a low reduction current on GCE/TNT/Pt and GCE/TNT/Pd due to the presence of the supported metals (Pt and Pd). SnO₂ in Sn-TNT can act as an active component via the formation of metal oxide solid solutions to enrich catalytic surface oxygen species and active sites [28]. This can assist in catalytic hydrogen production. A reductive process occurred on GCE/Sn-TNT/Pt and GCE/Sn-TNT/Pd in 0.1 mol L⁻¹ H₂SO₄. Drive currents of 0.148 mAcm⁻² and 1.32 mAcm⁻² were measured on screen printing at 0.258 V and 0.249 V, respectively. These values are slightly higher than the driven current determined for Sn-TNT, as shown in Table 1. The supported metals (Pt and Pd) on the enriched nanocomposite Sn-TNT allow for efficient electrocatalysis, leading to their superior HER activity with a lower onset overpotential of 0.220 V with a high current density, 3.239 mAcm⁻², than for each metal individually (Table 1).

Table 1. HER kinetics parameters obtained by analysis of CV and linear Tafel polarization curves for TNT and Sn-TNT catalysts.

Electrode	Cyclic Voltammetry		Linear Tafel Polarization	
	I (mA/cm ²)	-E(mV)	-j _o (mA/cm ²)	-j (μA/cm ²) at -400 mV
GCE	-	-	1.1803	0.136
CGE/TNT	-	-	1.215	0.510
CGE/TNT/Pt	0.143	258	1.22846	155
CGE/TNT/Pd	1.003	252	1.2697	571
CGE/TNT/Pt-Pd	3.406	232	1.3651	2530
CGE/Sn-TNT	0.05611	280	1.21832	0.883
CGE/ Sn-TNT/Pt	0.148	258	1.255031	198
CGE/ Sn-TNT/Pd	1.32	249	1.30405	1457
CGE/ Sn-TNT/Pt-Pd	3.239 mA	220	1.331594	2135

In comparing the CVs of GCE/TNT/Pt-Pd and GCE/Sn-TNT/Pt-Pd, although the undoped TNTs create a high reduction current, the Sn-TNTs/Pt-Pd catalyst is superior in that it produces a similarly high current, but with less overpotential. The hydrogen cathodic current density produced by different catalysts was determined by the linear polarization curves in Fig. 4 and is summarized in Table 1. The same trend of HER electrocatalytic activity was observed as was seen in the CV measurements. The activity of various TNT and Sn-TNT catalysts towards the HER was evaluated from the linear polarization curves in Fig. 4 recorded in 0.1 mol L⁻¹ H₂SO₄. The corresponding

hydrogen cathodic current density ($-j_o/\text{mA}/\text{cm}^2$) results are given in Table 1. A difference in activity between the TNTs and the Sn-TNT catalyst is clearly observed.

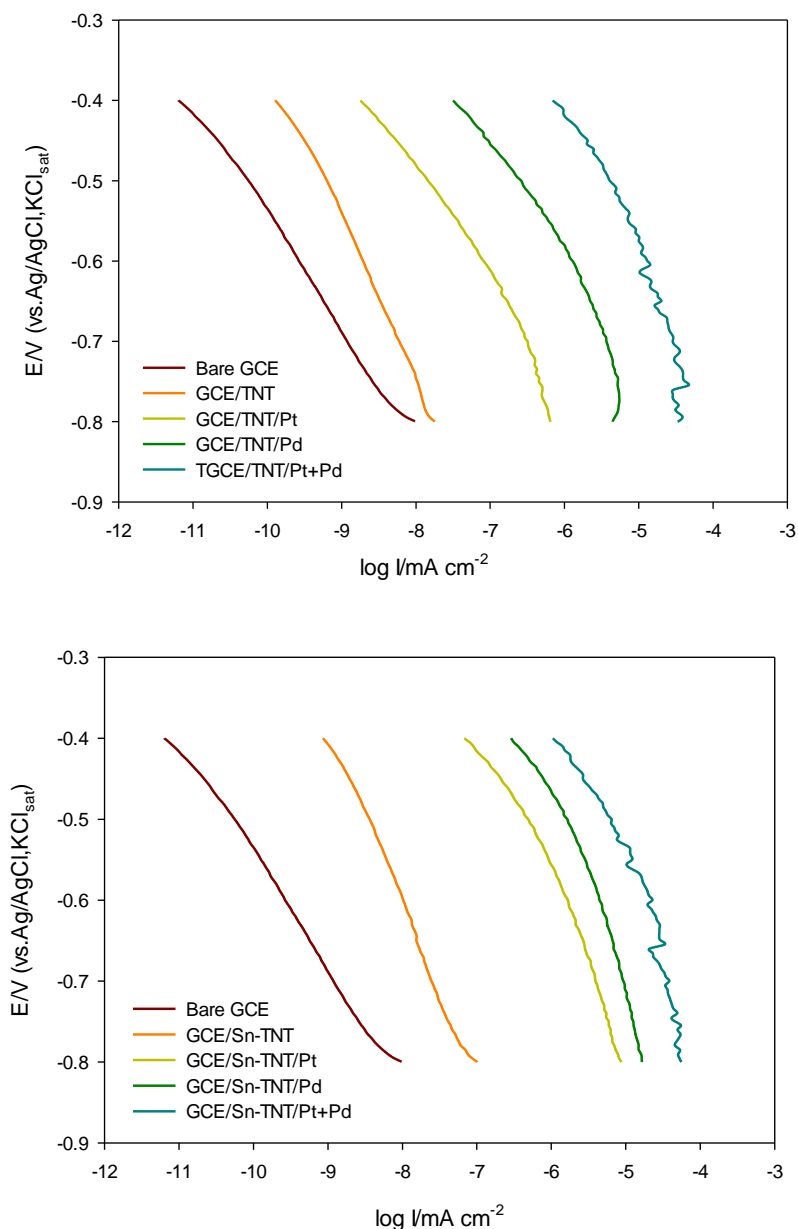


Figure 4. Tafel plots of TNTs and Sn-TNTs in $0.1 \text{ mol L}^{-1} \text{ H}_2\text{SO}_4$.

To better compare the HER activity of synthesized catalysts, one must understand that the HER does not occur at a reversible potential, but instead requires a certain overpotential. The measured exchange current density ($-j/\mu\text{A}/\text{cm}^2$) at -400 mV in Table 1 reveals the same order of electrocatalytic activity.

In general, modification of the surface and bulk properties of titanium oxide through doping with impurities is an effective way to improve electrochemical properties. Metal doping electron

and/or hole traps can appear in the surface or bulk phase of TiO₂ due to metal doping, which then improve the electron–hole pairs in the catalyst. At the same time, it can hybridize the new valence band of TiO₂ and the dopant. This leads to a narrowing of the band gap. Additionally, when new catalyst materials are developed for the HER, it is crucial that the catalyst exhibit a free energy of adsorbed atomic hydrogen that is close to equilibrium with the free energy of gaseous H₂. This is because the strength of the hydrogen binding will control the elementary step of the HER. This may increase free energy along the reaction pathway and decrease catalytic activity [9,10,13,14,31].

Furthermore, improvements in electrochemical kinetic behavior occur through increased electron conductivity that facilitates the charge transfer kinetics at the solid-liquid interface [31,43].

A plausible reaction mechanism of hydrogen production was suggested. Traditionally, the mechanism of the HER in acidic media is assumed to proceed by an initial formation of hydrogen intermediates (H_{ads}), which occurs *via* charge-induced discharge of protons or water ($\text{H}^+ + [\text{H}_2\text{O}] + \text{e}^- \leftrightarrow \text{H}_{\text{ads}} + [\text{OH}^-]$); this is the so-called Volmer step. This is accomplished either by the Tafel reaction, $2\text{H}_{\text{ads}} \rightarrow \text{H}_2$, or by transfer of a second electron in the Heyrovsky reaction, $\text{H}_2 \rightarrow \text{H}_{\text{ads}} + \text{H}^+ + \text{e}^-$. At low current densities the charge transfer (Heyrovsky reaction) is a slow step, while at higher current densities the protonation of the organic base (Tafel reaction) become the slow one [44].

The shape of the Tafel curves in Fig. 4 for TNTs and Sn-TNTs suggests a diffusion-limited reaction controlled by mass transport through narrow pores in the tubular structures of the catalysts. The mean values of the Tafel slopes for TNT and Sn-TNT (190 mV.dec⁻¹ and 210 mV.dec⁻¹, respectively) suggest that the HER on these catalysts follows the Volmer-Tafel mechanism, where the rate of the first electron transfer is included with the hydrogen adsorption step as the rate-determining step.

Based on the experimental and characterization results, a plausible reaction mechanism was proposed for the GCE/Sn-TNTs/Pt-Pd bimetallic supported catalyst that accounts for improved H₂ evolution (Fig. 5). The mechanism is based on the direct conduction pathway provided by the TiO₂ nanotubes and the co-catalytic role of Sn, Pt, and Pd on TNTs. As shown in Fig. 5, Sn is dispersed in the TNT lattice, and Pt and Pd are well deposited on the surface of the Sn-TNTs. The excited electrons in the conduction band (CB) of TiO₂ jump to active sites in co-catalyst SnO₂. These electrons are easily transferred to the supported metals and readily trapped by their vacant *d* orbitals before they recombine with holes. H⁺ is reduced to H₂ by the excited electrons. Minimized electron–hole recombination may be possible through the trapping of electrons by Pt and Pd metals and holes by a SnO₂ scavenger. The variation of spurted metals may provide multiple sites for electron exchange, and thus the Sn-TNTs/Pt-Pd catalyst provides excellent performance for the HER.

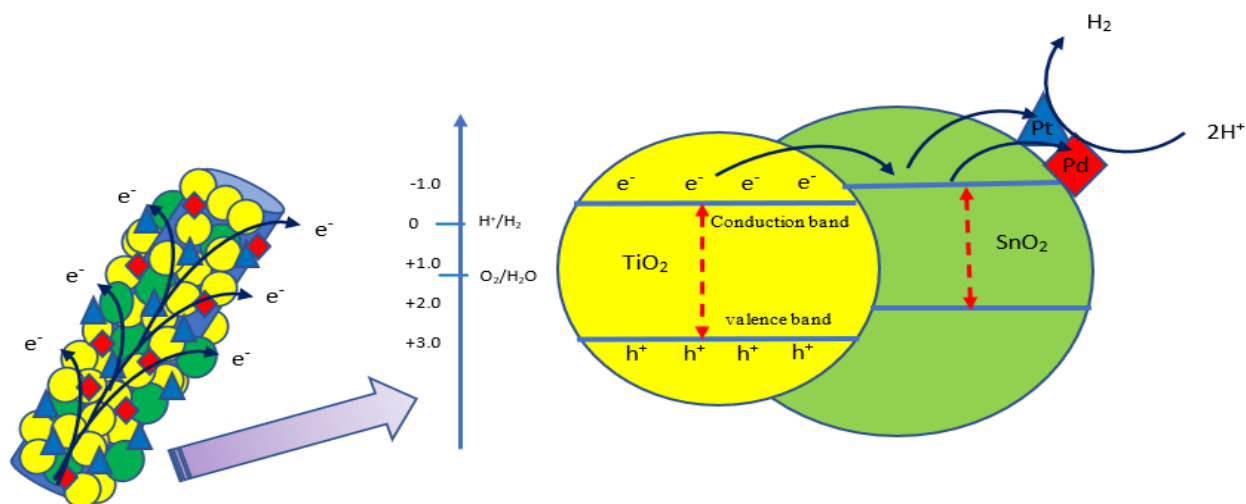


Figure 5. Mechanism of electro-generated charge separation in Sn-TNT/Pt+Pd.

According to CVs and linear polarization data, the exceptional performance and high electrocatalytic activity of the TNT/Pd and Sn-TNT/Pd cathodes are attributed to the abundance of Pd active sites with optimized atomic hydrogen binding energy for the cathodic HER. Volcano plots, which predict metals with an optimal H-binding energy, have been used as guides to tailor HER catalysts in acidic media. At the apex of the plot are the noble metals Pt, Ir, and Pd, which have nearly identical activities [30, 45, 46]. Based on the metal– H_{ad} energetics of these two elements in the observed volcano relationship, Pt has less metal– H_{ad} energy than Pd, but the smaller radius of Pd (4d) may lead to it being more adhesive to the semiconductors (in our case, TiO_2 and SnO_2) and thus more quickly accepting the excited electron.

3.3. Activation Energy

Before the reactants can be converted into products, the free energy of the system must overcome the activation energy (E_a) for the reaction. To determine the activation energy of the HER on TNT/Pt-Pd and Sn-TNT/Pt-Pd, DC linear polarization (Tafel) measurements were taken over a wide temperature range, from 303 K to 348 K, in $0.1 \text{ mol L}^{-1} \text{ H}_2\text{SO}_4$. Fig. 6 shows a set of Tafel curves recorded on the GC electrode modified with TNT/Pt-Pd and Sn-TNT/Pt-Pd at various temperatures.

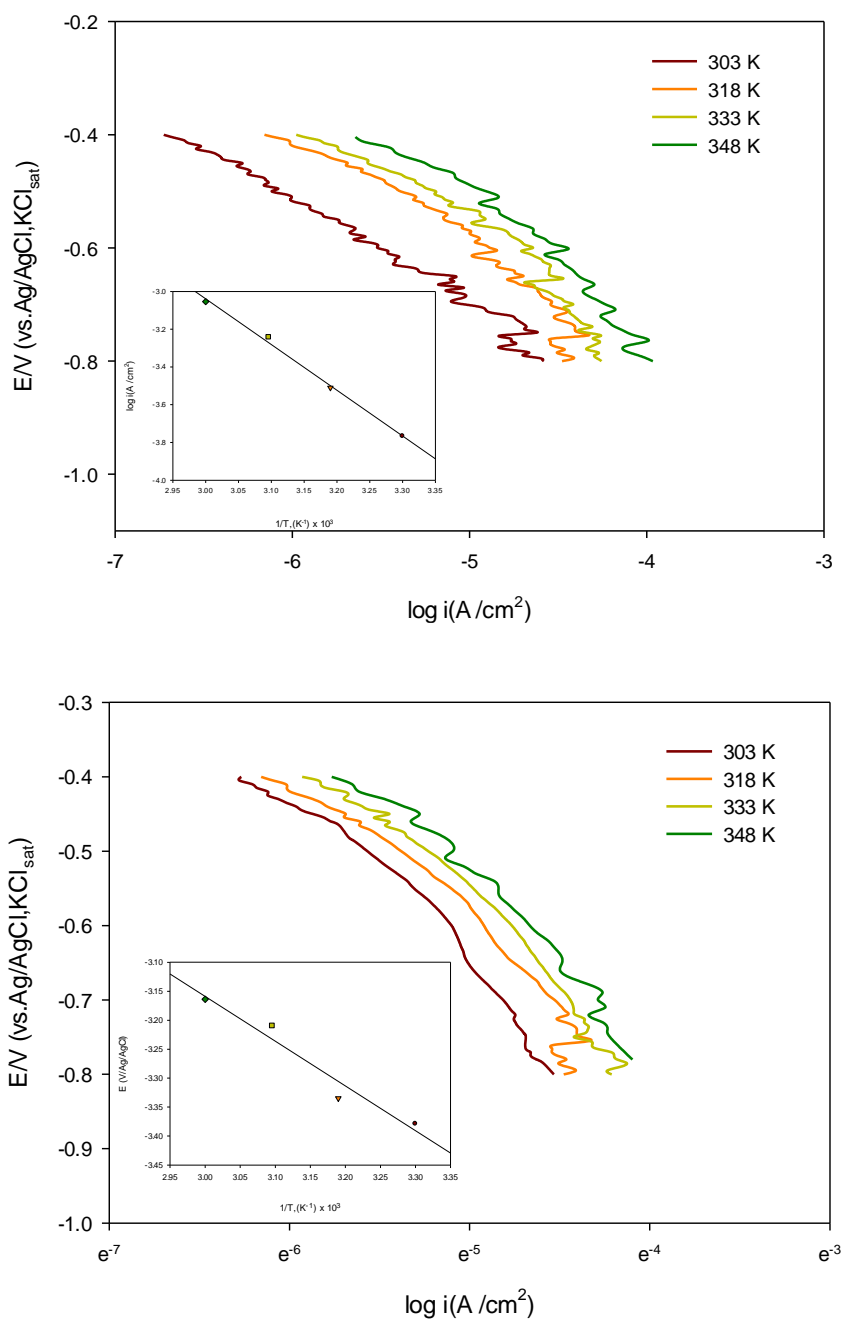


Figure 6. Linear Tafel polarization curves for the HER recorded on GCE modified with (a) TNT/Pt+Pd, (b) Sn-TNT/Pt+Pd in 0.1 mol L⁻¹ H₂SO₄ at various temperatures, *inset* Arrhenius plot for the HER.

The Arrhenius plot inset in Fig. 6 demonstrates that the cathodic current increase was linear in a semilogarithmic plot, i.e. the Arrhenius equation. The high Tafel slopes for the HER on TNT/Pt-Pd (≈ 196 mV/dec) and Sn-TNT/Pt-Pd (≈ 215 mV/dec) confirm the Volmer-Tafel mechanism in both solutions. The rate-limiting step does not change with temperature [47]. The apparent activation energy for the HER was calculated from the slope of the line in the Arrhenius plot. The lower activation energy calculated for hydrogen ion discharge ($E_a=2.78$ kJ/mol) on the Sn-TNT/Pt-Pd catalyst

compared with that on TNT/Pt-Pd ($E_a=8.75$ kJ/mol) indicates that active sites at the Sn-TNT/Pt-Pd catalyst surface are much more active than terrace sites in free TNT. The presence of hybrid metal as Sn^{4+} creates hybrid nanomaterials that improve the proton reductive doping of TNT and modify its energy gap properties.

As we mentioned, loading elements into hydrothermally synthesized TiO_2 nanotubes plays an important role in their activity properties.

Table 2. Activation energy variation for different catalysts.

Catalyst	Activation energy, $\text{kJ}\cdot\text{mol}^{-1}$	Solution	Ref.
TNT/Pd	9.23	0.1 mol L^{-1} H_2SO_4	[14]
Sr-TNT/Pd	5.56	0.1 mol L^{-1} H_2SO_4	[14]
Undoped TNTAs	10.79	0.1 mol L^{-1} H_2SO_4	[13]
Nd-Pt-TNTAs	3.53	0.1 mol L^{-1} H_2SO_4	[13]
Gd-Pt-TNTAs	3.11	0.1 mol L^{-1} H_2SO_4	[13]
Nd-Gd-Pt-TNTAs	2.02	0.1 mol L^{-1} H_2SO_4	[13]
Pt-TNTAs	5.87	0.1 mol L^{-1} H_2SO_4	[13]
TNT/Pt-Pd	8.75	0.1 mol L^{-1} H_2SO_4	This study
Sn-TNT/Pt-Pd	2.78	0.1 mol L^{-1} H_2SO_4	This study

A comparison of the activation energy of the HER on other TNT catalysts is summarized in Table 2 under the same conditions. Incorporation of metal ions into the TiO_2 matrix and the use of Pt group metals as an outer layer improved the electrocatalyst efficiency. Sn as the dopant and Pt/Pd as the cosupported catalyst led to superior performance compared to Sr ions and single Pt catalysts. On the other hand, it was clearly observed that anodized synthesized nanotube arrays had lower E_a values. Self-organized and vertically oriented TiO_2 nanotube arrays provide a better system for electron transfer.

4. CONCLUSION

In this study, the focus was on the cathode side, which is the site of the hydrogen reaction. Factors influencing the effectiveness of the HER were studied to develop TNT and Sn-TNT catalysts

prepared by hydrothermal methods in the anatase phase. The introduction of SnO₂ into the TiO₂ lattice could narrow the band gap and create an enriched catalyst with active sites. The improved performance of the Sn-TNTs/Pt-Pd catalyst and its low activation energy ($E_a=2.78$ kJ/mol) could be attributed to the supported metals in the surface area endowed by the hollow structures and numerous nanopores within the shell. The hydrogen adsorption energy ($M-H_{ads}$) of Pt and Pd plays a crucial role in cosupported catalysts. Finally, we use the activation energy of the HER to directly compare the electroactivity of test catalysts. This work may serve as a framework for future semiconductor electrocatalyst heterojunction designs that depend on more than just Pt, which has a high market price, for enhanced electrocatalytic applications.

ACKNOWLEDGMENTS

The authors thank Prof. Abdullah Al-Mayouf from King Saud University for his helpful advice on various technical issues. In addition, the authors would like to thank the technicians, Mr. Abdallah Jaber (Physics Department) and Miss. Roa'a Abo Saif (Chemistry Department) for conducting surface measurements of the study samples.

AUTHORS' CONTRIBUTIONS

Emran and Alsahli, who are the corresponding authors, participated in the overall experiments. Both authors read and approved the final manuscript.

COMPETING INTERESTS

The authors declare that they have no competing interests.

References

1. Y. Qiu, W. Chen, S. Yang, *Angew. Chem. Int. Ed.*, 122 (2010) 3757.
2. G. I. N. Waterhouse, A. K. Wahab, M. Al-Oufi, V. Jovic, D.H. Anjum, D. Sun-Waterhouse, J. Llorca, H. Idriss, *Sci. Rep.*, 3 (2013) 2849.
3. M. Abdullah, S. K. Kamarudin, L.K. Shyuan, *Nano. Res. Lett.*, 11(2016) 553.
4. S. Yang, H. Lee, *Nano. Res. Lett.*, 12 (2017) 582.
5. T. Kasuga, M. Hiramatsu, A. Hoson, T. Sekino, K. Niihara, *Langmuir*, 14(12) (1998) 3160.
6. T. Kasuga, *Thin Solid Films.*, 496(1) (2006) 141.
7. A. Fujishima, K. Honda, *Nature*, 238 (1972) 37.
8. Y. Jiangdong, G. Cheng, W. Zhi, W. Yongneng, X. Wang, S. Yufeng, S. Lan, L. Changjian, *J. Mater. Chem. A*, 3 (2015) 22218.
9. E. C. Su, B. S. Huang, M. Y. Wey, *Solar Energy*, 134 (2016) 52.
10. N. L. Reddy, S. Kumar, V. Krishnan, M. Sathish, M. V. Shankar, *J.Catal.*, 350 (2017) 26.
11. E.U. Lačnjevac, R. Vasilić, T. Tokarski, G. Cios, P. Žabiński, N. Elezović, N. Krstajić, *Nano Energy*, 47 (2018) 527.
12. P. K. Dubey, R. Kumar, R. S. Tiwari, O. N. Srivastava, A. C. Pandey, P. Singh, *Int. J. Hydrog. Energy*, 43 (2018) 6867.
13. K. M. Emran, H. E. Alanazi, *J. Exp. Nanosci.*, accepted, 2021.
14. K. M. Emran, *Int. J. Electrochem. Sci.*, 15 (2020) 4218.
15. M. Epifani, J. D. Prades, E. Comini, E. Pellicer, M. Avella, P. Siciliano, G. Faglia, A. Cirera, R. Scotti, F. Morazzoni, J. R. Morante, *J. Phys. Chem. C*, 112 (2008) 19540.
16. Y. F. Sun, F. C. Lei, S. Gao, B. C. Pan, J. F. Zhou, Y. Xie, *Angew Chem Int Ed*, 52 (2013) 10569.
17. T. Zeng, P. Ji, X. Hu, G. Li, *RSC Adv.*, 6 (2016) 48530.

18. Y. Yanga, H. Li, H. Zhao, R. Qu, S. Zhang, W. Hu, X. Yu, X. Zhu, S. Liu, C. Zheng, X. Gao, *J. Hazard. Mater.*, 371 (2019) 156.
19. F. Mueller, D. Bresser, V. S. K. Chakravadhanula, S. Passerini, *J Pow Sourc.*, 299 (2015) 398
20. G. D. Park, J. K. Lee, Y. C. Kang, *J. Mater. Chem. A*, 5 (2017) 25319.
21. G. Zhang, M. Liu, *Sens. Actuators B*, 69 (2000) 144.
22. C. Li, Z. Yu, S. Fang, S. Wu, Y. Gui, R. Chen, *J. Physics: Conference Series*, 152(2016) 012033.
23. Y. Wei, J. Liu, F. Cheng, J. Chen, *J. Mater. Chem. A*, 7 (2019)19651.
24. I. Rangel-Vazquez, G.D. Angel, V. Bertin, F. Gonzalez, A. Vazquez-Zavala, A. Arrieta, J.M. Padilla, A. Barrera, E. Ramos-Ramirez, *J. Alloy Comp.*, 643 (2015) S144.
25. X. Zhu, L. Pei, R. Zhu, Y. Jiao, R. Tang, W. Feng, *Sci. Rep.*, 8 (2018)12387.
26. H. Zhuang, Y. Zhang, Z. Chu, J. Long, X. An, H. Zhang, H. Lin, Z. Zhang, X. Wang, *Phys. Chem. Chem. Phys.*, 18 (2016) 9636
27. A. Sengele, D. Robert, N. Keller, C. Colbeau-Justin, V. Keller, *Appl. Cataly. B: Enviro.*, 245 (2019) 279.
28. Y. H. Li, H. Zhao, R. Qu, S. Zhang, W. Hu, X. Yu, X. Zhu, S. Liu, C. Zheng, X. Gao, *J. Hazard. Mater.*, 371 (2019) 156.
29. E. Skúlason, V. Tripkovic, M. E. Björketun, S. Gudmundsdóttir, G. Karlberg, J. Rossmeisl, T. Bligaard, H. Jónsson, J.K. Nørskov, *J. Phys. Chem. C*, 114 (2010)18182
30. N. Danilovic, R. Subbaraman, D. Strmcnik, V. R. Stamenkovic, N. M. Marković, *J. Serb. Chem. Soc.*, 78 (12)(2013) 2007.
31. J. Durst, C. Simon, F. Hasché, H. A. Gasteiger, *J. Electroche. Soci.*, 162 (1) (2015) F190
32. B. E. Conway, G. Jerkiewicz, *Electrochim. Acta*, 45 (2000)4075.
33. S. Afshar, M. Hakamizadeh, *J Exp. Nanosci*, 4(1) (2009)77.
34. M. R. Kulish, V. L. Struzhko, V. P. Bryksa, A. V. Murashko, Il'in V G 2011 Hydrothermal synthesis and properties of titania nanotubes doped with Fe, Ni, Zn, Cd, Mn, *Semicond. Phy. Quantum Electron. Optoelectron.* 14 (1) 21.
35. K. M. Emran, S. M. Ali, H. E. Alanazi, *J. Electroanal.Chem.*, 856 (2020)113661.
36. N. Harsha, K. R. Ranya, K. B. Babitha, S. Shukla, S. Biju, M. L. P. Reddy, K. G. K. Warriar, *J. Nanosci. Nanotechnol.*, 11 (2011)1175.
37. E. C. Su, B. S. Huang, M. Y. Wey, *Solar Energy*, 134 (2016) 52.
38. T. Vu. H. Au, L. Tran, T. Nguyen, T. Tran, M. Pham, M. Do, D. Nguyen, *J. Mater. Sci.*, 49 (2014) 5617.
39. K. M. Emran, H. E. Alanazi, Fabrication and Characterization of Lanthanide-TiO₂ Nanotube Composites, submitted.
40. A. Kusior, J. Klich-Kafel, A. Trenczek-Zajac, K. Swierczek, M. Radecka, K. Zakrzewska, *J. Eur. Ceram. Soc.*, 33 (2013) 2285.
41. B. Tahir, M. Tahir, N. A. S. Amin, *Energ. Convers. Manage*, 15 (2018) 9284.
42. L. C. Chen, F. R. Tsai, S. H. Fang, Y. C. Ho, *Electrochim. Acta*, 54 (2009) 1304.
43. M Zhang, J. Wu, J. Hou, J. Yang, *Sci. Adv. Mater.*, 5 (6)(2013) 535.
44. R. Crețu, A. Kellenberger, M. Medeleanu, N. Vaszilcsin, *Int. J. Electrochem. Sci.*, 9(2014) 4465.
45. JO'M. Bockris, *J. Serb. Chem. Soc.*, 70 (3)(2005) 475.
46. N. Dubouis, A. Grimaud, *Chem. Sci.*, 10 (2019) 9165.
47. Z. Tang, L. Liao, Y. Zheng, J. Kang, Y. Chen, *J. Chem. Phys.*, 25(4) (2012) 469.